ELSEVIER

International Journal of Mass Spectrometry 212 (2001) 535–551

www.elsevier.com/locate/ijms

Implementation of low-energy surface-induced dissociation (eV SID) and high-energy collision-induced dissociation (keV CID) in a linear sector-TOF hybrid tandem mass spectrometer

Eugene N. Nikolaev[a,1], Árpád Somogyi[a], Darrin L. Smith[a], Chungang Gu[a], Vicki H. Wysocki[a,*] Charles D. Martin[b,2], Gary L. Samuelson[b]

[a] *Department of Chemistry, University of Arizona, Tucson, AZ 85721, USA;*
[b] *JEOL USA, Inc., Peabody, MA, USA*

Received 3 April 2001; accepted 3 May 2001

Abstract

In the work reported here, an in-line sector-TOF (time-of-flight) tandem mass spectrometer with a coaxial detector was developed. An advantage of the present design is that the instrument implements both high-energy collision-induced dissociation (keV CID) and low-energy surface-induced dissociation (eV SID) with no hardware manipulations required to switch between the two activation methods. Surface characterization by secondary-ion mass spectrometry is also possible with this design. Gas phase collision-induced dissociation in this sector-TOF requires ion gating of the continuous ion beam and an ion buncher to bring the ions into spatial focus at the focal-point "source" of the offset parabolic field reflectron. The offset parabolic field reflectron provides good resolution over virtually the entire product ion mass range, with no need to step the reflector voltages. For surface-induced dissociation experiments, accomplished with a surface placed after the last reflectron electrode, the electrodes that comprise the CID reflectron are used for deceleration and acceleration of the ion beam before and after it collides with the surface, respectively. The results obtained show successful implementation of keV CID and eV SID in a JEOL HX110A/TOF mass spectrometer. Product ion mass accuracy is better than ±0.4 u for keV CID and ±0.1 u for eV SID. Typical resolutions achieved are 8000–12,000 (for selected ions), 1000 (for keV CID fragments), and 300–400 (for eV SID fragments). This difference in the CID and SID resolution is partially the result of the different total flight times in CID and SID experiments. On the basis of a direct comparison of keV CID and eV SID of protonated leucine enkephalin, SID experiments have a lower detection limit than CID experiments by at least an order of magnitude. (Int J Mass Spectrom 212 (2001) 535–551) © 2001 Elsevier Science B.V.

1. Introduction

In recent years, time-of-flight (TOF) mass analyzers have become popular in many applications, including their use as the second analyzer in tandem mass spectrometers. This application is the result of the high sample-use efficiency possible with TOF analyzers as well as high sensitivity, good mass accuracy and resolution, and a large *m/z* range. TOF mass analysis is deceptively simple: flight times of ions are monitored and related to their *m/z* values by the simple kinetic energy expression, $E = mv^2/2$. As pointed out in the foreword to Cotter's book on TOF mass spectrometry [1], the implementation is not as simple as the concept. Recently, however, great im-

* Corresponding author. E-mail: vwysocki@u.arizona.edu.

[1] On leave from the Institute of Energy Problems for Chemical Physics of the Russian Academy of Sciences, Moscow, Russia

[2] Present address: Applied Biosystems, 500 Old Connecticut Path, Framingham, MA 01701, USA

Dedicated to R. Graham Cooks on the occasion of his sixtieth birthday.

PII S1387-3806(01)00462-6

provements in TOF capabilities have occurred [1–3], spurred by advances in fast electronics and detection [2] as well as by the need to couple the high mass range of TOF with matrix-assisted laser desorption/ionization (MALDI) sources [1,4]. In the work described here, a TOF mass analyzer was added to a traditional JEOL HX 110A double-focusing EB sector instrument (electric, E, sector coupled to magnetic, B, sector) to serve as the second analyzer in a tandem mass spectrometer. The JEOL sector instrument is a workhorse instrument that is used to obtain accurate mass measurements for reaction products of synthetic chemists. It was desired to extend the capabilities of this instrument to tandem mass spectrometry for both structural characterization and gas phase chemistry studies. The implementation of high-energy (keV) CID provides an established and reproducible activation method that results in a broad range of fragment ion types. In addition, sectors operate at kV acceleration voltages that are compatible with TOF analysis. The unique feature of the current design, which has a surface installed after the last electrode of the reflectron, is the implementation of the surface-induced dissociation (SID) method on the same tandem instrument with no changes in hardware. SID provides a versatile activation method that has been shown to deposit relatively narrow distributions of internal energy [5] and high average internal energies [5] and, thus, excellent control over internal energy. Surface-induced dissociation is not currently available on commercial mass spectrometers, and its successful implementation with reasonable resolution in this prototype instrument is a step toward its implementation in commercial TOF systems.

High-energy CID, low-energy CID, and SID have been implemented in a wide range of instrument types over the years, and all are useful activation methods that play a role in tandem mass spectrometry [5–10]. It is not within the scope of this article to review these techniques and their various implementations in a variety of instrument types; readers are referred to a number of reviews on these topics [5–10]. Rather, we focus on addition of a TOF analyzer with high-energy CID and low-energy SID capabilities to a commercial JEOL HX110A EB sector instrument. The TOF design is an offset parabolic reflector with a coaxial detector. Other sector-TOF designs for high-energy CID have been proposed or presented in the literature: they include both orthogonal and in-line designs [11–18] as well as the curved field reflectron design of Cotler and Cornish [16]. Note that none of the previous designs use the offset parabolic reflector. One BE sector-TOF for SID has recently appeared in the literature [19,20].

2. Experimental

2.1. Instrument setup

A schematic diagram of the in-line sector/TOF instrument is shown in Fig. 1. A more detailed drawing of the TOF analyzer illustrating the CID cell and SID surface is shown in Fig. 2. The buncher indicated in Fig. 2 is set to 0 V for the SID experiments. Pulse timing for the ion gate and buncher was controlled with a Stanford Research Instruments (Sunnyvale, CA) DG535 digital delay generator. Spellman HV (high-voltage) Electronics (Plainview, NY) power supplies were used for most HV supplies, and Behlke HV switches (Eurotek, Morganville, NY) were used for HV pulsing.

The precursor ions, mass and energy selected by the sector instrument, enter the TOF analyzer through the exit slit of the sector. Methods of ionization employed in this work include FAB (fastatron bombardment with the conventional Xe gun of the JEOL HX110A) and EI (70 eV electron impact ionization). The vacuum chamber of the sector is separated from the TOF by an isolation valve, and the sector instrument can be used independent of the TOF. After entering the TOF chamber, the ion beam is focused by a pair of quadrupolar lenses in such a way that a rectangular (slit) shape beam leaving the sector is compressed into an almost circular ion beam. The quadrupolar lens focusing method is the same for both high-energy CID and low-energy SID. It is important to note here that the only differences between the CID and SID experimental settings are the voltages and pulse-timing parameters, i.e., no rearrangement in the

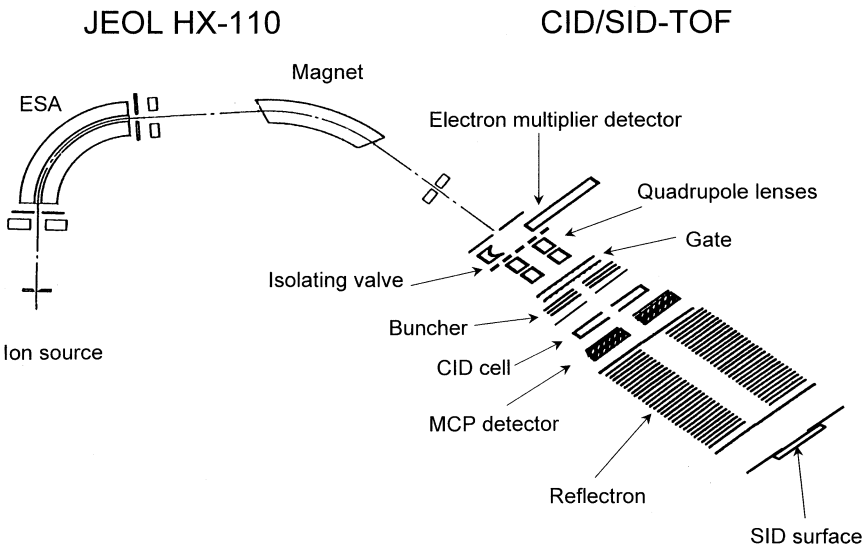

Fig. 1. General schematic of the in-line JEOL sector-time-of-flight instrument.

hardware in the vacuum chamber is necessary. Separate descriptions and discussions of the two ion-activation experiments are presented below.

A PC running Windows 3.1 and JEOL TOF software was used for spectra acquisition and mass analysis. In keV CID, the mass axis was calibrated internally with a simple two-point calibration using two fragments of known masses. In keV CID, mass accuracy was typically better than ±0.4 u for both precursor and fragment ions. The CID resolution

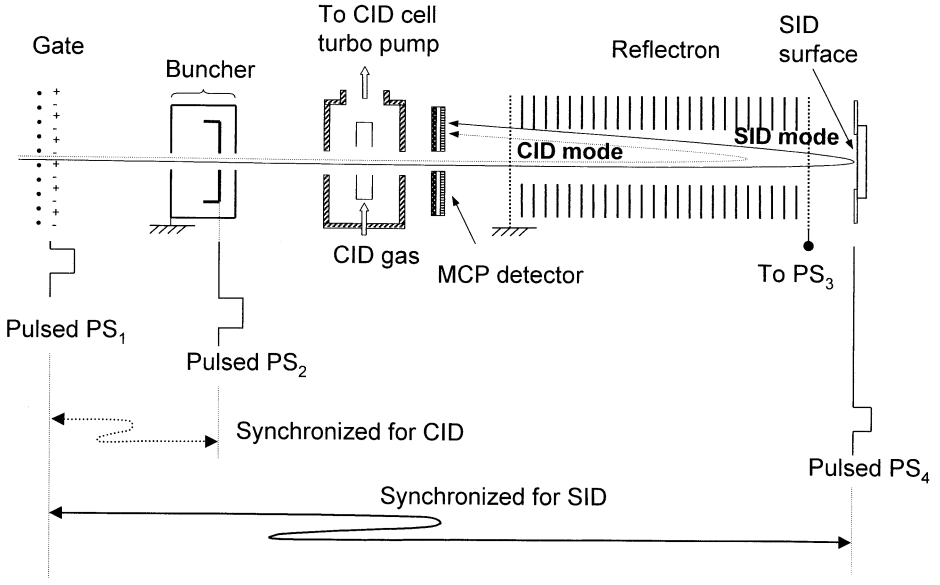

Fig. 2. Detailed schematic of the time-of-flight analyzer used to perform both high-energy collision-induced dissociation and low-energy surface-induced dissociation experiments.

appears to be limited by the accuracy of the reflectron field in the CID mode; the reflectron spacers in this prototype instrument are made of a compressible material (Teflon), so they are not identical widths and will be replaced in future work. Note that in the SID mode, the ions were not turned around in the reflectron field, and mass accuracy ($\pm$0.1 u) was improved over CID. In this case, the parent ion and a known fragment can be used for calibration. Over a million TOF acquisitions were typically summed to obtain spectra. (With a typical duty cycle of 5000 Hz, the collection and accumulation of 1,280,000 spectra is possible in 256 s.)

2.2. High-energy (keV) CID experiments

After leaving the quadrupolar lenses, the continuous ion beam is modulated in both space and energy [1,22]. An ion gate [17,22] and buncher combination is used to select a packet of ions from the continuous ion beam. The ion gate is an "interleaved comb", or bipolar design consisting of a series of parallel wires. The bipolar ion gate is normally energized with alternate $+/-$ voltages on each grid wire, deflecting the ion beam away from the buncher. The required potential applied to the alternating wires is determined by the mass of the selected ions and the acceleration voltage. Typically, the voltages used in our experiments were $\pm$200–250 Volts. The grid wires used were 0.3-mm-diameter wires spaced 1 mm apart horizontally. To begin an experiment, the ion gate voltage is pulsed off (i.e., set to 0 V), allowing ions to pass through the gate for a period of time sufficient in duration to allow the ion buncher to fill with precursor ions. Typical times required ranged from 200 ns to 2 μs, depending on the *m/z* (and, thus, the velocity) of the precursor ion. The time required to fill the buncher is also dependent on the velocity of the precursor ions and the length of the buncher and is, therefore, dependent on both the acceleration voltage and the *m/z* of the precursor ions. Correct values for the ion packet length were calculated using MathCAD and stored as a table for easy reference. The most commonly used buncher length in our tests was 4 cm, requiring that the ion gate select an ion packet of slightly less than 4 cm in length.

A variety of buncher designs were tested to optimize the buncher for the planned CID experiments. Initial experiments with multielectrode bunchers were less than optimal because of electric field inhomegenieties and high interelectrode capacitance. The required high-speed pulsing of the buncher was complicated by the presence of interelectrode capacitance that discharged slowly through the resistor dividers required in multielectrode geometries. Buncher lengths of 8–25 cm were constructed where each electrode was pulsed down with a diode; however, the peak shapes obtained with these longer bunchers were, again, less than ideal. The final design of the shaped field ion buncher was accomplished by modeling a nonlinear, gridless, two-electrode, 4-cm-long, fully shielded, shaped electrode buncher in SIMION. Electrode shapes were experimentally adjusted for optimum spatial focus of the ion packet at the focal point of the reflectron. Although in SIMION the theoretical temporal width of the ion packet at the spatial focal point was $<$1 ns, actual minimum peak widths at full width half maximum (fwhm) in our experiments with precursor ions were hardware limited to 2–3 ns.

The shaped-field two-electrode buncher (Fig. 2) modulates the ion energy in such a way that the ions arriving first lose more energy than do those arriving later. The entrance electrode of the buncher is at ground potential, and the exit electrode of the buncher is held at a fixed voltage during the period of time when the buncher is filling with ions. Deceleration of an ion is determined by the potential applied to the exit electrode and the penetration depth of the ion into the buncher. When the lead ions in the ion packet reach the exit electrode, the exit electrode is pulsed to 0 V, thus assigning a modulation value to the ions depending on each ion's position within the buncher. The ions in the lead of the ion packet will then have a lower velocity than the ions at the back of the packet. The point at which the trailing ions reach the lead ions will be the spatial focal point, and this is determined by the magnitude of the modulating potential at a fixed ion-source acceleration potential.

Ideally, this focal point should be the location of the coaxial MCP detector and also the focal point (virtual source) of the reflectron. The required buncher voltage pulse is dependent on the acceleration voltage, the *m/z* of the precursor ions, and the length of the field-free drift region. The buncher focal point is independent of the mass of the ions. In our experiments, at 10 kV acceleration, the buncher voltage required to produce the desired focal point was 1100 V. The field-free-region distance from the buncher to the focal point was typically 750 mm.

The collision cell in our instrument is located before the coaxial ion detector, ~600 mm downstream from the buncher. The position of the CID cell is, in practice, not critical. If a very small kinetic energy release during dissociation is ignored, the velocity of the fragment ions will be very nearly the same as that of the parent ion. Therefore, the position of the temporal focusing point for both the parent and fragments is the same. It is desirable to locate the CID cell far enough away from the reflectron entrance to reduce ion decomposition in the reflectron region. The collision cell is a small volume of a few millimeters in length and is located in a differentially pumped section of the vacuum chamber. In high-energy CID experiments, the collision cell is filled with a collision gas (which, in most cases, was He, but occasionally was N_2). Gas flow was controlled with a needle valve. The most effective method of determining the collision gas pressure for optimum CID was to adjust the gas flow for the maximum *S*/*N* of the product ions. Alternatively, the collision gas flow could be adjusted by increasing the flow until the precursor ion signal was attenuated by ~60%–70%. Either method worked equally well. In experiments using FAB ionization of CsI (*m/z* 912 cluster), similar CID spectra were obtained both when using the CID cell and without the cell, which was removed from the vacuum chamber—that is, with the entire differentially pumped region several centimeters in length flooded with He. It was apparent in this experiment that the limit of the resolution of the fragment ions was not determined by the location of the dissociation, as long as the dissociation was in the field-free region between the exit aperture of the buncher and the entrance to the reflectron.

After dissociation of the parent ion, an offset parabolic field reflectron is used to compensate for the considerable energy distribution of the precursor and fragment ions created by the gate-buncher combination. The offset parabolic field reflectron (i.e., a truncated parabolic field with a short linear segment at the entrance) permits the detection of fragment ions without degradation of resolution because the temporal focal point of the reflectron is not dependent on the mass of the fragment. Product ions of a very wide mass range will all have the same temporal focal point. The reflectron is comprised of 100 equally separated, disc-shaped electrodes. The reflectron plates are connected to a resistive voltage divider that provides individual voltages to each of the electrodes. Alternative reflector designs have also been considered. However, only the offset parabolic reflectron design provides the unique ability to focus the product ions without regard to the modulation energy spread introduced by the ion buncher. Another advantage of this reflectron design is a relatively long field-free region between the reflectron and the detector. The field created by such a reflectron is cylindrically symmetric, an ideal match for our beam shape and annular detector shape. Importantly, the inclusion of a field-free region in the temporal focal length of the offset parabolic reflectron allows for the space required to locate the CID cell in front of the coaxial MCP detector that is required to be at the focal point. The fixed voltage applied to the reflectron must be slightly higher than the sector acceleration voltage to insure that all product ions (in the singly charged case) that enter the reflectron are turned around inside the reflectron and accelerated back to the coaxial detector. In most of our CID experiments, the reflector voltage (PS3; Fig. 2) was set to 120% of the acceleration voltage.

Although only EI and FAB results are presented in this article, we note here that the experiments are not restricted to the investigation of singly charged ions. Electrospray ionization (ESI) has been used to investigate a limited number of multiply protonated peptides. Of course, for keV CID, the charge state of the

selected ion is limited by the maximum high voltage applied to the reflectron. In our instrument, this value is 15 kV, which means that for 5 kV operation of the sector (which is default for ESI), the maximum charge state for primary ions is three. In principle, a triply charged ion can decompose to generate a singly charged ion, the mass and velocity of which are very close to that of the precursor. As a consequence, this singly charged ion has an energy that is close to an energy three times the acceleration voltage (requiring a reflectron voltage >15 kV). In principle, higher charge states can be investigated by lowering the acceleration voltage on the sector instrument (lower than 5 kV), but this leads to lower ion signal (i.e., decreased sensitivity). In conjunction with one of our recent studies, the high-energy CID spectra of the ESI-generated singly and doubly protonated peptides (e.g., RLDIFSDF and LDIFSDFR) have been recorded and published (reference [23] and its supplementary material). The occurrence and dominance of *y* ion formation from $[LDIFSDFR+2H]^{2+}$ in the sector-TOF instrument are very similar to the Q-SID-Q results [23].

The ions temporally focused by the reflectron are detected by the MCP detector positioned coaxially with the primary ion beam. The coaxial MCP detector assembly has a center aperture to allow the primary ion beam to pass through it. Initial experiments using an offset conical anode MCP detector were degraded by wide peaks (3–4 ns fwhm) and ringing. The manufacture of the offset conical anode detector was also complicated and expensive. In later experiments, a prototype, flat-anode, high-speed MCP detector developed by Hammamatsu, Bridgewater, New Jersey (after consultations with JEOL USA), was used. This flat-anode detector design is capable of producing presursor ion peaks with subnanosecond fwhm. Experiments using a LeCroy (Chestnut Ridge, NY) 8-GHz Digital Storage Oscilloscope (DSO) revealed consistent precursor ion peaks of <2 ns fwhm.

The acquisition system used in both CID and SID modes includes a 1-GHz multiple-stop time-to-digital converter, TDC, (Precision Instruments, model 9805). The minimum peak fwhm detectable by this model TDC is 3.0 ns. The parent ion peaks from the flat-anode detector were typically on the order of 1.5 ns fwhm as measured on a digital oscilloscope, thus requiring the addition of some low-pass filtering before the MCP detector signal is passed to the TDC input. Mini-Circuits (Brooklyn, NY) low-noise amplifiers and low-pass filters were used to provide the 100-mV threshold, 3.0-ns-fwhm signal required by the TDC. As the TDC operates on the principle of a start and stop signal, it has virtually zero noise, and it is, therefore, possible to sum many hundreds of thousands of acquisitions without the accumulation of systematic noise. The acquisition rate was limited primarily by the TOF of the precursor ion and was typically 4–5 kHz.

2.3. Low-energy (eV) SID experiments

The change to SID mode from CID is accomplished by disconnecting and connecting cables to the signal generator followed by fine tuning to optimize the SID signal. In addition, the gas flow to the CID collision cell is turned off and the buncher voltage is set to zero. The surfaces used in the SID experiments are self-assembled monolayers (SAMs) of fluorinated alkanethiols on gold (i.e., $CF_3(CF_2)_9(CH_2)_2S$-Au). The SID surface is located ~13 mm beyond the end of the reflectron. The energy modulation of the ion packet provided by the buncher in CID cannot be corrected in the SID mode because in the SID mode, the ions are not turned around in the reflectron and, thus, no energy correction is possible. Indeed, in the SID mode, the electrodes of the "reflectron" are used to generate a deceleration field for the parent ions before the collision with the surface and as an offset parabolic acceleration region for the product ions after collision. This design is similar to that described by Duncan and coworkers for photodissociation [24]. The voltage on the exit electrode of the reflectron is lowered to a value slightly less (by ~125–200 V) than the value of the sector acceleration voltage. This allows the nearly monoenergetic and mass-selected precursor ions to pass completely through the reflectron electrodes so as to strike the SID surface. Monoenergetic precursor ions are important for studies of dissociation mechanisms, which are one focus

of our laboratory. (Precursor ions arriving at the SID surface with substantial kinetic energy distributions would lead to uncertainty in the SID collision energy but might be exploited in the future to give a range of collision products useful in practical analytical application of SID.)

Initially, sputtered peaks from the fluorinated alkanethiolate surface (*m/z* 31 and 69) were seen in the SID spectra. The sputtered ions proved to be the result of surface sputtering caused by high-energy neutrals formed in the last field-free region of the sector (between the magnet and the entrance slit of TOF). The ion gate cannot modulate these fast-moving neutrals. As a consequence, they continuously struck the surface, and sputtered ions were accumulated in the surface/reflectron region. These sputtered ions were swept out, together with "real" SID fragment ions, when the surface potential was pulsed. The intensities of the sputtered ions were independent of the reflectron and surface voltages and were proportional to the primary ion beam intensity. The "neutral-generated" sputtered ions were completely eliminated by tilting the TOF axis by about 2^0 with reference to the last field-free region of the sector.

The ion packet from the ion gate is decelerated to 150–200 eV (for singly charged ions) through the reflectron electrodes (now being used as a deceleration region) and allowed to travel past the last electrode of the reflectron so as to strike the surface. The entrance and exit electrodes of the reflectron contain grids to reduce distortions in the electric fields within the reflectron. (Note that the current coarse grids will be replaced with fine grids in future to further minimize field distortion.) The precursor ion collision energy with the surface (i.e., the SID collision energy) can be controlled by adjustment of the potential difference between the ion source (acceleration potential) and the surface (surface potential). Both the acceleration voltage and the surface voltage can be measured with reasonably high accuracy, but slight changes in energy of the precursor ions because of fine tuning of the repeller and focusing lenses must be assumed (e.g., no more than ± 5 V). Nevertheless, zero collision energy can be well predicted by fine adjustments of the surface potential. Obviously, there is an upper limit: If the surface potential is higher than the acceleration potential (including repeller and lens voltages), ions will be reflected back without hitting the surface. The precursor ion peak is, therefore, shifted to a slightly shorter time. Collision energies of 10–100 eV (with reference to this "turning" potential) were common values in our experiments.

After a short delay of a few hundred nanoseconds, the SID surface potential is pulsed up to a repulsion voltage (Fig. 3) to eject the ions resulting from the surface collision back to the reflectron. Thus, in SID experiments, the reflectron is used only to decelerate the sector-selected precursor ions and accelerate the SID product ions. The voltage applied to the SID surface is controlled by two power supplies (a high-voltage power supply providing a constant but adjustable surface potential and an additional pulsed power supply, PS_4). This relatively low-voltage pulse ($\sim$500 V) is added to the constant surface potential and used to sweep out and focus SID product ions from the vicinity of the surface back through the reflectron to the detector.

The timing of this surface pulse is critical and must be carefully synchronized with the gate pulse. If the time delay between the gate and the surface pulse is too short, ions from the "back tail" of the ion packet will not hit the surface and may be forced to turn back. (Although not shown, in some of our experiments a peak at higher *m/z* than that of the selected ion appears in our SID spectra. This peak is associated with parent ions that have not yet reached the surface when the extraction pulse is applied. The peak is the result of nonideal synchronization of the gate pulse and the surface extraction voltage pulse; that is, these ions are leftover ions that are electrostatically reflected by the increased surface potential. The intensity of these peaks depends on the accuracy of synchronization.) If, however, the delay time between the gate and the surface pulses is too long, the fragment ions may be too far away from the surface and cannot be focused efficiently. A time limit for the surface pulse delay is determined by the length of the ion packet and the kinetic energy of the fragments departing from the surface. The (time and/or spatial) width of the precursor ion packet can be controlled by

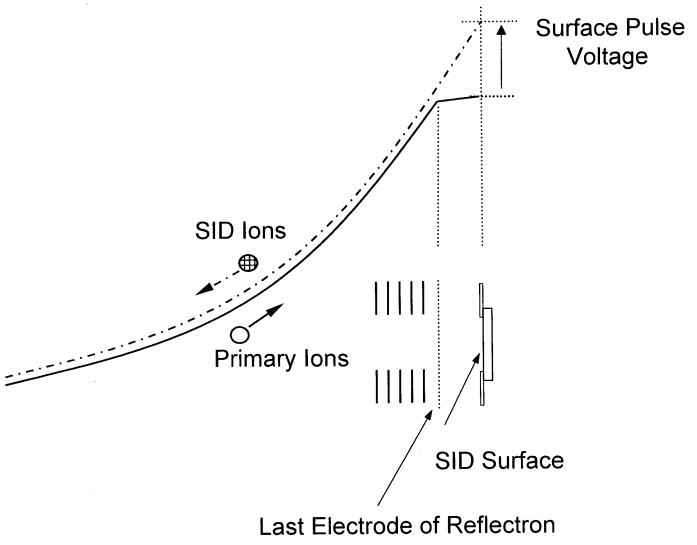

Fig. 3. Pulsed delayed extraction of surface-induced dissociation (SID) ions in the SID mode of operation. Solid curve indicates the potential profile for precursor ions. Dot-dashed curve indicates the potential profile for SID ions. After a short delay following the ion–surface collisions, the SID surface potential is pulsed up to a repulsion voltage to eject the ions from the surface back into the reflectron.

the gate pulse (which has a minimum pulse with of 200 ns). On the basis of recent results by Hanley and coworkers [25], we can assume that the fragment ions do not leave the surface with high kinetic energy (e.g., at a 50 eV collision, this energy is likely $<$10 eV). However, because the surface potential is slightly higher than the potential of the last electrode of the reflectron, the fragment ions are immediately accelerated towards the reflectron (see Figs. 2 and 3). As a consequence, we generate an ion beam of SID ions with both velocity and spatial distribution. By applying an appropriate surface pulse with a synchronized delay, that is, a type of a delayed extraction, one can focus the SID ions. For a 50 eV collision of benzene-d_6 molecular ion, the potential difference between the surface and the last electrode of the reflectron is $\sim$60 V. If we assume, for example, that the fragment at *m/z* 56 is formed close to the surface, it can gain an average energy of 30–35 eV between the surface and the last reflectron electrode. For a fragment of *m/z* 56 with 35 eV average kinetic energy, it takes $\sim$900 ns to pass through the distance of 13 mm between the surface and the last reflectron electrode. For $C_6D_6^{+\cdot}$, our experience shows that a typical surface pulse delay time of 18.2 μs gives an SID spectrum with well-focused precursor and fragment ions (see, e.g., Fig. 7 below), but a delay time of 18.6 μs leads to defocused $C_2D_2^{+\cdot}$, $C_2D_3^+$, and $C_3D_3^+$ fragment ions. Thus, changes of 300–500 ns in the surface-pulse delay can result in differences in the SID spectra consistent with the predictions of the simple model above. The offset parabolic field reflectron further accelerates the product ions in combination with the SID surface pulse potential (as indicated by the dot-dashed curve of the potential profile; Fig. 3), bringing the product ions into temporal focus at the surface of the coaxial MCP detector.

3. Comparison and Discussion of high-energy CID and low-energy SID spectra

3.1. Fragmentation spectra of selected projectile ions

The keV CID and eV SID performance of the instrument first was tested by dissociation of CsI clusters. Fig. 4a shows the high-energy CID spectrum

of *m/z* 1692. (The sector acceleration voltage was 10 keV in this experiment.) The TOF ion peak width of the sector-selected precursor ion (without the collision gas) lead to a calculated TOF resolution of $t/\Delta t$ = 12,000. (For other sector-selected ions, TOF resolutions of 8000–12,000 have been measured.) In the CID experiment, the peak widths for CID product ions were in the range of 15–100 ns, which provided at least unit resolution in the entire mass range. As can be seen in Fig. 4, the peak width for the fragment of *m/z* 912 is 32 ns, which corresponds to a calculated resolution of 1060.

The 30-eV SID spectrum obtained by collision of the CsI cluster of *m/z* 1692 with a fluorinated SAM surface is shown in Fig. 4b. By comparison with Fig. 4a, it is clearly seen that eV SID provides more extensive fragmentation than does keV CID, consistent with a higher average internal energy deposition for SID. Although the absolute peak widths are similar in both the keV CID and eV SID spectra (32 and 40 ns for *m/z* 912, respectively), the calculated resolution for the SID fragment ions is significantly lower than for CID ions (380 versus 1060 for *m/z* 912; Fig. 4). The lower calculated resolution is because of the fact that the time of flight of SID ions is about one-half that of the CID ions because they are referenced to the surface pulse ($t = 0$). (As will be demonstrated below, e.g., in Fig. 5, this does not prevent separation of fragment ions one mass unit apart, i.e., achieving unit resolution for SID fragments.)

Note that, in some experiments, SID spectra have also been obtained without the use of the TOF parabolic accelerating field. For clarification, remember that the reflectron electrodes are used to decelerate the parent ions before the surface collision and then to accelerate the SID product ions. The 30-eV SID spectrum of singly charged YGGFL (FAB ionization) obtained with the acceleration/deceleration reflectron electrodes completely removed from the system shows, for example, that the sensitivity for SID ions in this setup is similar to that with the parabolic acceleration field but the resolution is about three to four times worse than that achieved with the parabolic acceleration field (spectrum not shown).

The keV CID spectrum of protonated leucine enkephalin is shown in Fig. 5a. (The sector acceleration voltage was 5 keV in this experiment.) The b_3/y_2 (*m/z* 278/279) "doublet" is separated. The mass accuracy of the fragments in this experiment is better than ±0.4 u, so all fragment ions can easily be assigned. The corresponding SID spectrum (30 eV) is shown in Fig. 5b. The b_3/y_2 pair is also resolved in this SID spectrum. As expected, SID provides more extensive fragmentation that is manifested in immonium ions (e.g., F, Y) with higher intensity. Higher-mass fragments (such as a_4 and b_4) can also be seen in Fig. 5b and their intensities increase with decreasing SID collision energy.

Protonated leucine enkaphalin was used to carry out sensitivity tests. Low-energy SID was found to be at least 10 times more sensitive than keV CID. In one experiment, 18 pmol of sample on the FAB probe tip was successfully used to obtain both keV CID and eV SID spectra (i.e., without reloading the sample). The lowest detection limit for protonated leucine enkephalin in this sector-TOF instrument was found to be 1.8 pmol loaded on the FAB tip for SID experiments (spectra not shown).

SID spectra of singly charged Angiotensin II are shown in Fig. 6a–c. The SID spectra of Fig. 6a and 6b were obtained at 45 and 65 eV SID collision energies, respectively, on the fluorinated alkanethiolate surface in the sector-TOF instrument. The comparison of the high-energy CID spectrum (figure not shown) and the sector-TOF-SID spectra of Fig. 6a and 6b indicates that there is no mass discrimination in our TOF-SID instrument. To demonstrate the mass accuracy of better than ±0.1 u, the list of fragments with theoretical and measured masses for the spectrum of Fig. 6b is presented in Table 1. It is also seen in Fig. 6a and 6b that a 20-eV increase in the SID collision energy almost eliminates the precursor ion and significantly increases the intensities of immonium ions. (For fragmentation efficiency curves, see below.) For another comparison, the 65-eV SID spectrum obtained on a Q-SID-Q instrument of the Wysocki lab [10,26] is also shown in Fig. 6c. Although the incident angle is significantly different in the two instruments (45° in the Q-SID-Q and 90° in the sector-TOF-SID instru-

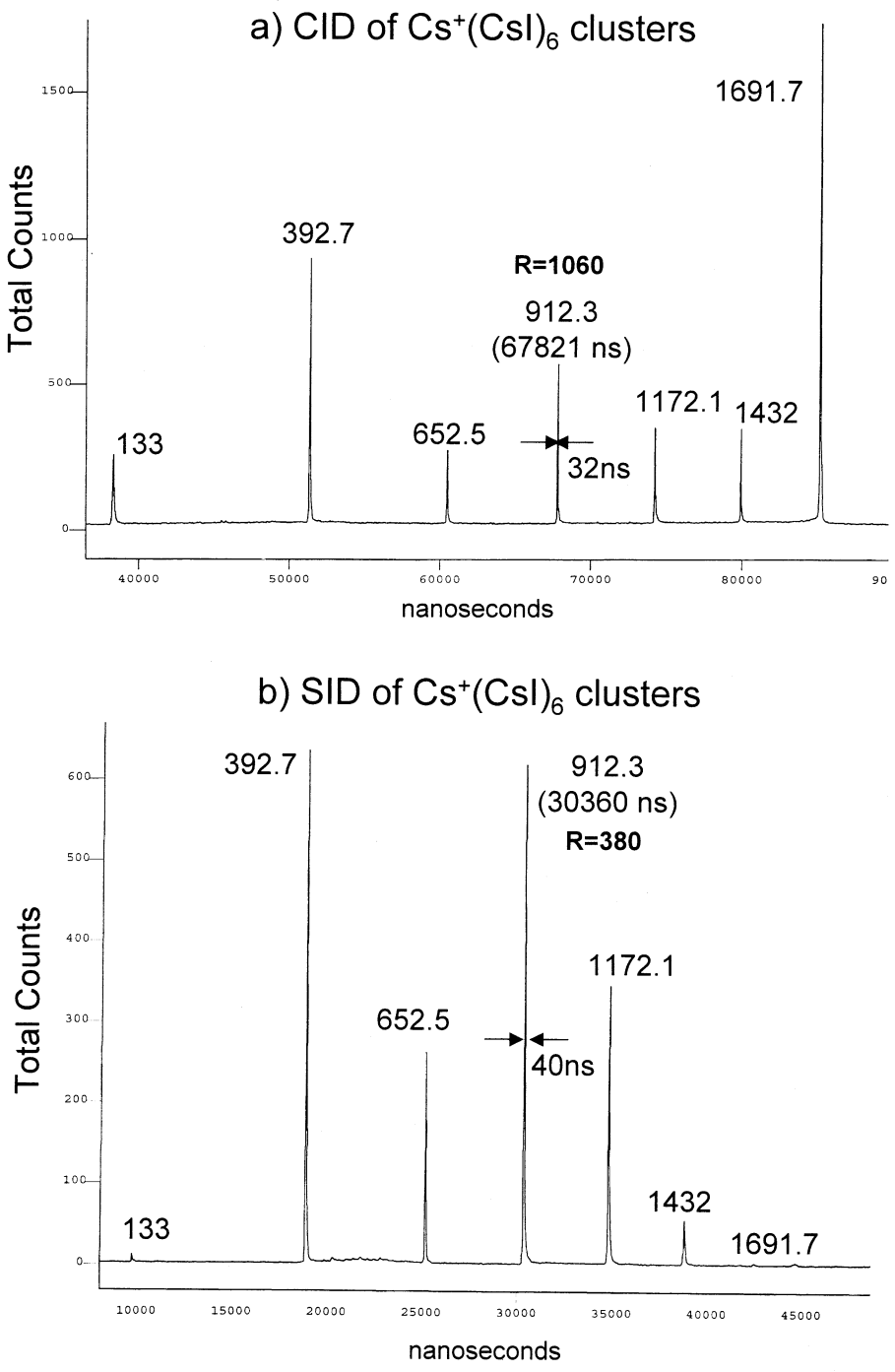

Fig. 4. (a) A 10 keV collision-induced dissociation spectrum of the CsI cluster at *m/z* 1692. The 32-ns peak width, time of flight, and resolution for the fragment *m/z* 912 are indicated (FAB ionization, pressure: 4×10^{-6} torr, collision gas: N_2). (b) A 30 eV surface-induced dissociation spectrum (fluorinated surface). The 40 ns peak width, time of flight, and resolution for the fragment m/z 912 are indicated.

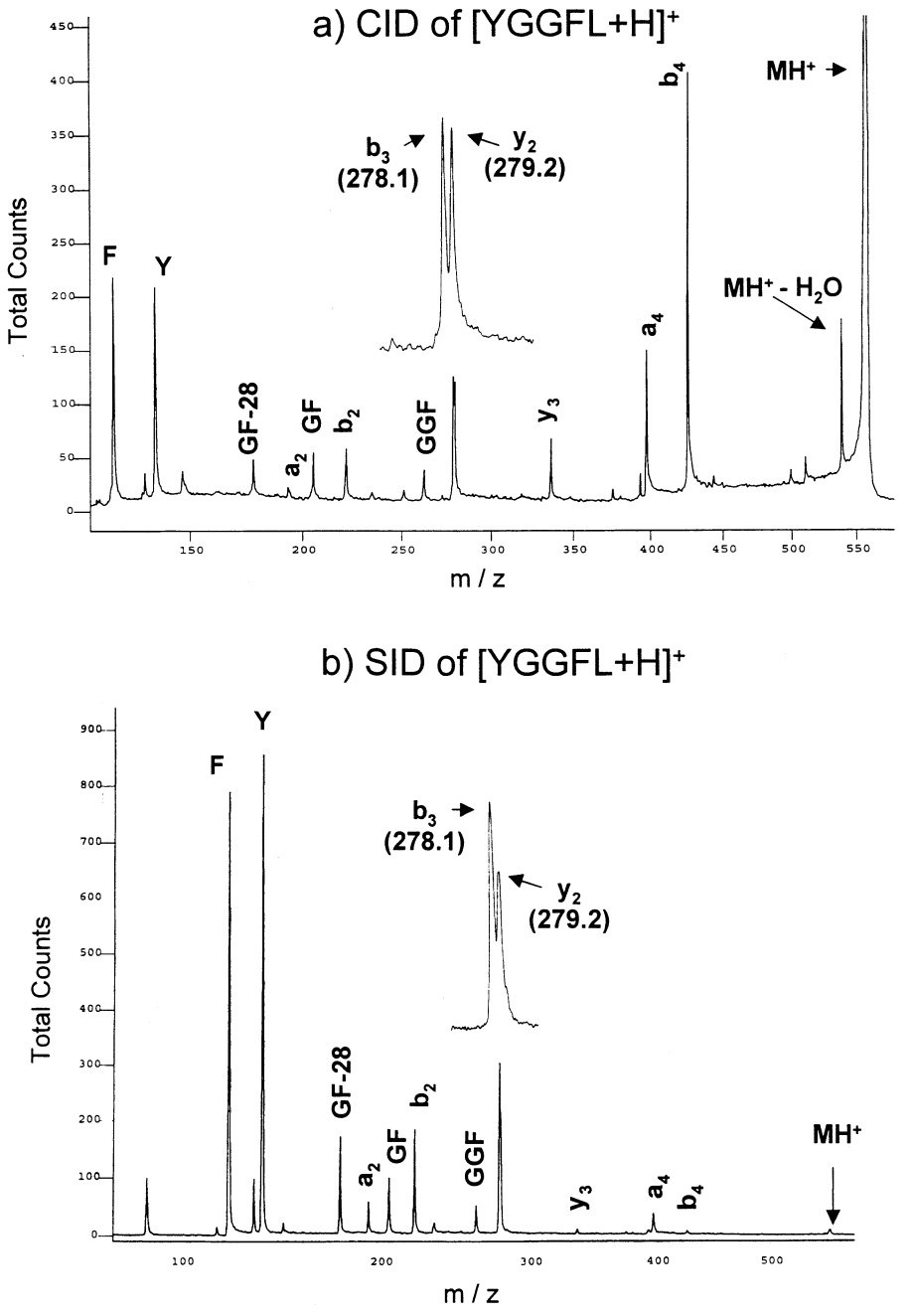

Fig. 5. (a) A 5 keV collision-induced dissociation spectrum of singly protonated YGGFL (FAB inization, pressure: 9.5×10^{-7} torr, collision gas: He). (b) A 30 eV surface-induced dissociation spectrum of singly protonated YGGFL (fluorinated surface).

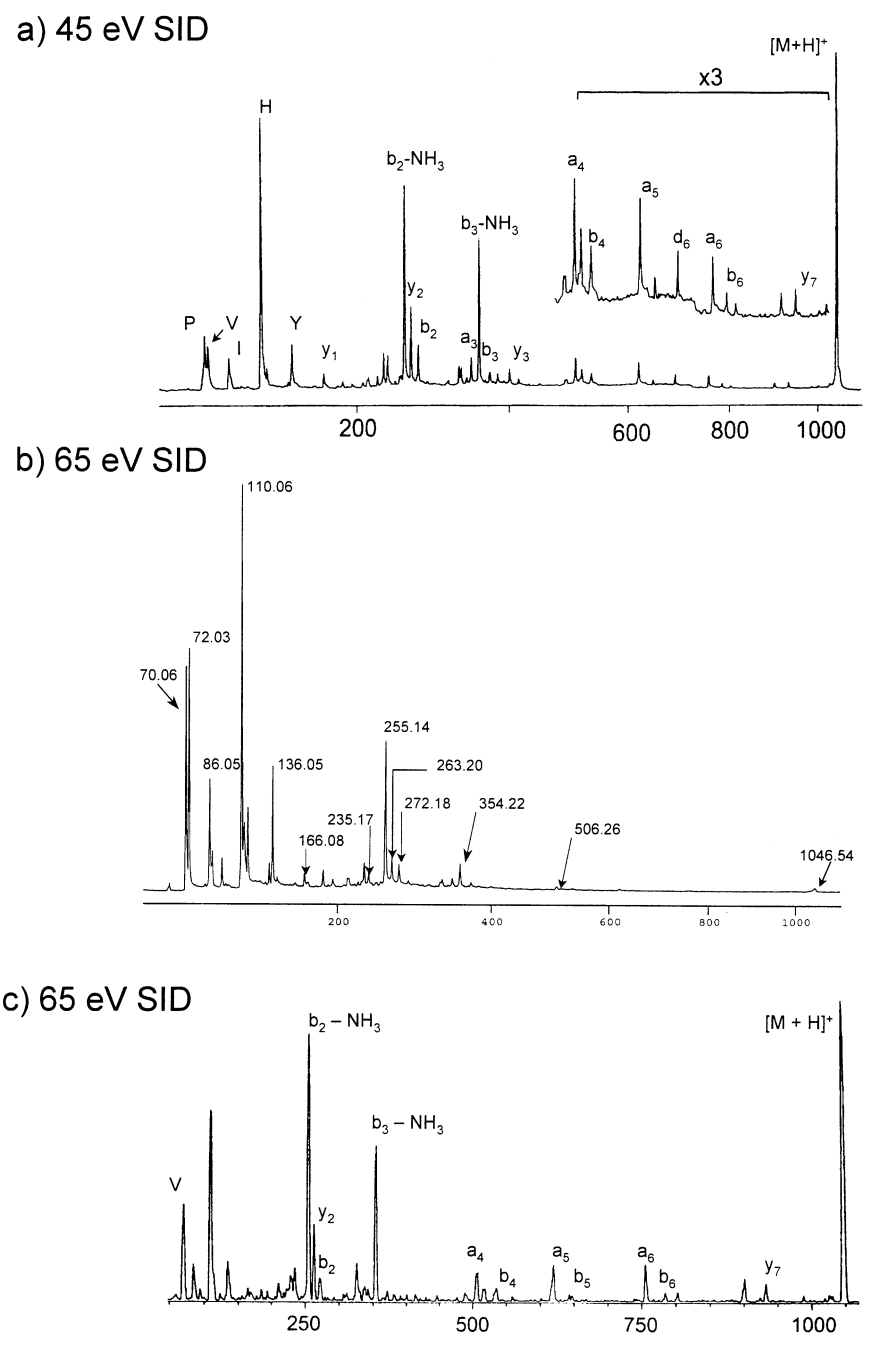

Fig. 6. SID (surface-induced dissociation) spectra of singly protonated Angiotensin II obtained at (a) 45 eV SID collision energy on the sector-time-of-flight (TOF)-SID instrument, (b) 65 eV SID collision energy on the sector-TOF-SID instrument, see peak assignments in Table 1 and (c) 65 eV SID collision energy on the Q-SID-Q instrument. All results were obtained by using fluorinated surfaces.

Table 1
Mass Accuracy SID Comparison Using Theoretical Values Calculated from MS-Product[a]

Ion	Theoretical m/z	Calibrated SID m/z	Difference
$[M + H]^+$	1046.54	1046.54	0.00
a_4	506.27	506.26	0.01
$B_3 - NH_3$	354.18	354.22	0.04
b_2	272.14	272.18	0.04
y_2 or VY	263.14	263.20	0.06
$B_2 - NH_3$	255.11	255.14	0.03
HP or VY − 28	235.12 or 235.14	235.17	0.05 or 0.03
y_1	166.09	166.08	0.01
Y	136.08	136.05	0.03
H	110.07	110.06	0.01
a_1	88.04	88.02	0.02
I	86.10	86.05	0.05
V	72.08	72.03	0.05
R or P	70.00 or 70.07	70.06	0.06 or 0.01

[a] Theoretical masses were taken from Protein Prospector: http://prospector.ucsf.edu.

ment), the general features of both spectra are similar. One difference between the Q-SID-Q and sector-TOF-SID spectra is that some additional ions, such as d_6, can be found in the TOF-SID spectrum. Note that in the Q-SID-Q experiment, singly charged Angiotensin II was generated by ESI ionization. The appearance of the d_6 ion can, therefore, be attributed to the higher internal energy deposition by FAB ionization, as previous work [26–28] has shown *d* ions to be stronger in SID when FAB ionization, rather than ESI, is used to produce parent ions. A systematic study is planned to reveal the features of the energy deposition function, the fragmentation characteristics (including fragmentation efficiency), and the role of FAB versus ESI ionization in SID experiments on the sector-TOF-SID instrument.

The 30 eV SID spectrum of benzene-d_6 molecular ion, *m/z* 84, obtained on the sector-TOF-SID instrument is shown in Fig. 7. (Benzene-d_6 molecular ions were generated by electron impact ionization at 70-eV ionization energy.) The SID spectrum shows the characteristic fragmentation pattern of benzene that has been obtained many times on the Q-SID-Q instrument [29–31]. Note that, similar to previous work [29–31], ion–surface reaction products can be detected at *m/z* 99 (C_6D_6+F–D_2) and 101 (C_6D_6+F–D). The origin of the fragment ions at *m/z* 28, 30, and 32 is not known at present, but it has recently been suggested that they originate from surface collision of an electronically excited state of benzene molecular ion [J.H. Futrell, private communication; 32].

The SID spectra of the molecular ion of acetone-d_6, *m/z* 64, obtained at 30- and 55-eV energies in the sector-TOF-SID instrument are shown in Fig. 8a and b, respectively. The spectrum in Fig. 8a is similar to that recorded earlier on the Q-SID-Q instrument [33]. Interestingly, there is a peak at *m/z* 66 that corresponds to a D addition to the molecular radical ion. It can be assumed that either some neutralized acetone or acetone fragments, adsorbed to the fluorinated surface, serve as the reaction partner to the selected molecular ion. (Acetone-d_6 is the only source of D in these experiments.) At higher energies (e.g., 55 eV and higher), fluorine-containing sputtered ions are detected (*m/z* 69, 100, 119, 131; Fig. 8b). This, and other experiments with Ar^+ and Xe^+ at >500 eV SID collision energy, indicate that another experiment type possible on this sector-TOF instrument is secondary ion mass spectrometry (SIMS) for characterization of surfaces.

3.2. Fragmentation efficiency curves

In addition to individual spectra, fragmentation efficiency curves ([fragment ion counts]/[total ion counts] vs. SID collision energy) [28,34] were ob-

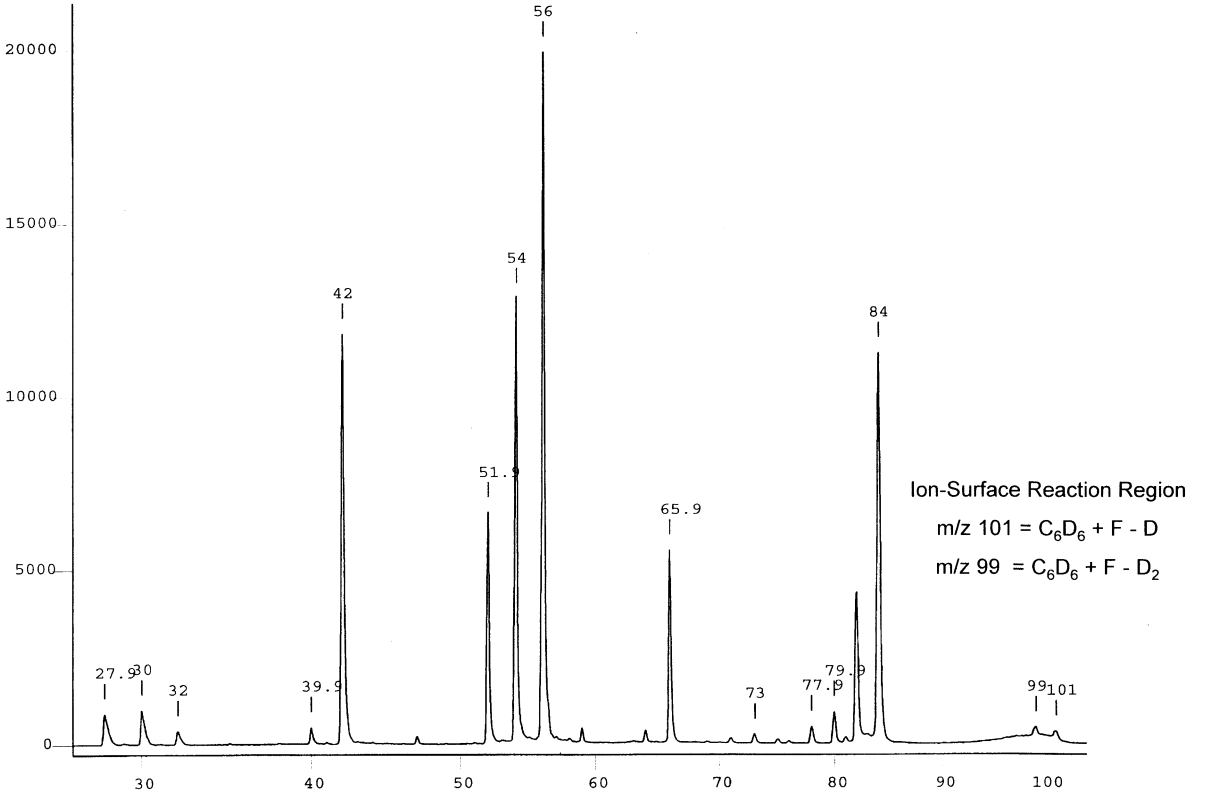

Fig. 7. A 30 eV surface-induced dissociation spectrum of benzene-d_6 molecular ion (fluorinated surface).

tained for several singly protonated oligopeptides (YGGFL, YGGFLR, YGGFLK, Angiotensin II, Bradykinin, Angiotensin I, Substance P, and Bombesin) colliding with the fluorinated surface. Fig. 9 shows representative curves for protonated leucine enkephalin (YGGFL), Angiotensin II (DRVYIHPF), and Angiotensin I (DRVYIHPFHL). A characteristic value of these logistic type curves is the inflection point, which was reproducible with an error of ± 4 eV. It is seen in Fig. 9 that peptides with increasing masses and increasing basicity require higher SID energy to fragment. The inflection point for YGGFL is 18.6 eV, which is close to the value of 19.2 eV [26] obtained on the Q-SID-Q instrument (45° incident angle) for the fluorinated surface. However, with increasing masses, the difference between the inflection point energies on the sector-TOF-SID and Q-SID-Q instruments increases. Additional and systematic studies, including the investigation of the effect of different ionization sources (FAB vs. ESI), are necessary to explain this trend. Nevertheless, general trends are reproducible that indicate that the sector-TOF-SID instrument can also be used to obtain fragmentation efficiency curves that are important in studies of energetics of peptide fragmentation.

4. Conclusions

An in-line sector-TOF tandem mass spectrometer was developed and tested in this work. High-energy CID and low-energy SID, as well as high-energy SIMS experiments, can be performed by using the same instrument setup. The only parameters to be changed are the voltages applied to the TOF ion optics and the acceleration voltage on the sector. All of these

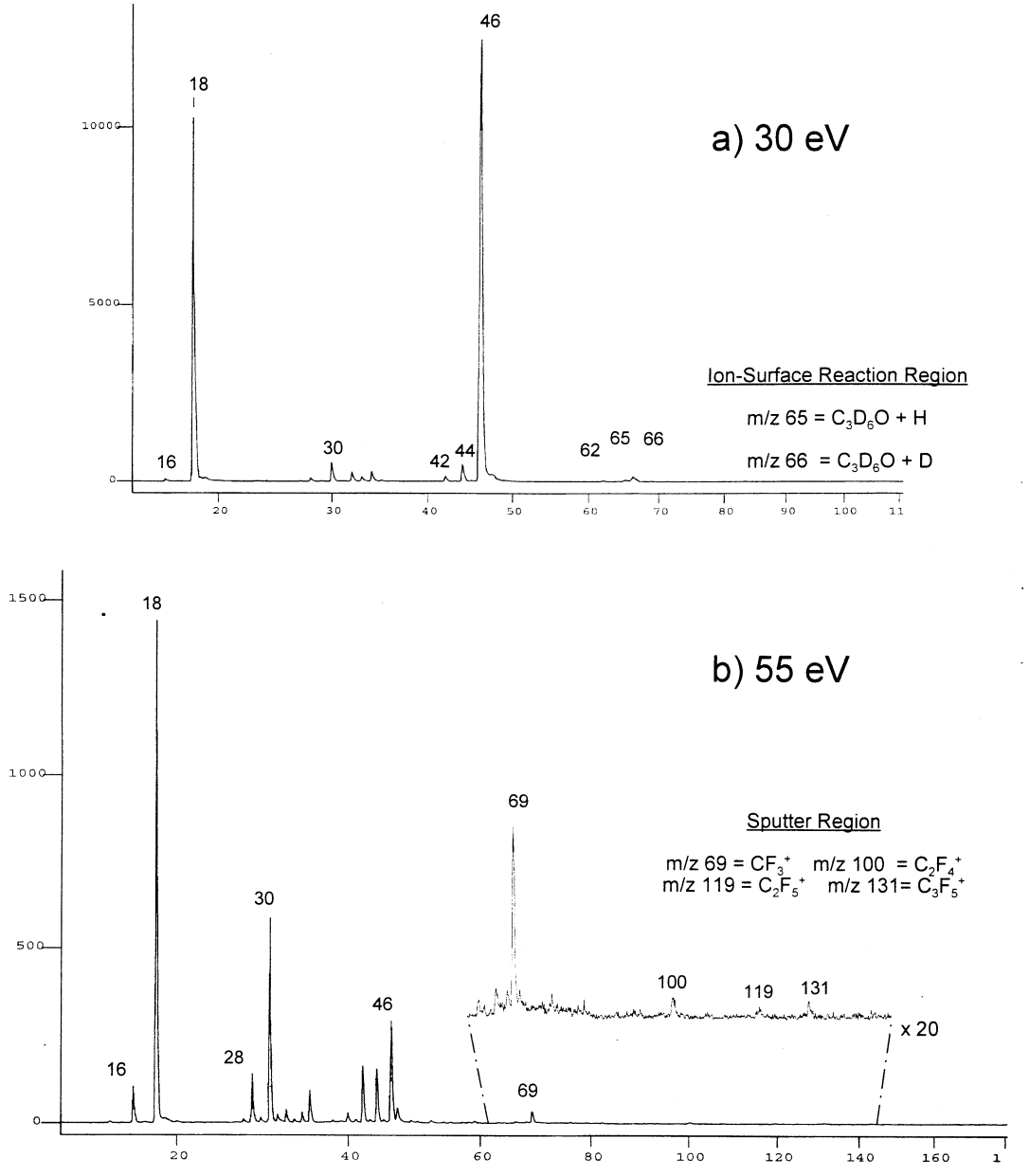

Fig. 8. SID (surface-induced dissociation) spectra of acetone-d_6 (fluorinated surface) at (a) 30 eV SID collision energy, and (b) 55 eV SID collision energy.

parameters can easily be varied, and switching between different modes of operation currently requires a reasonably short time. These operations could be fully automated and controlled by a computer program.

CID and SID spectra have been obtained for a variety of projectile ions generated by FAB and EI ionization methods. It has been demonstrated that the resolution is more than unit resolution over a relatively wide mass range for both CID and SID frag-

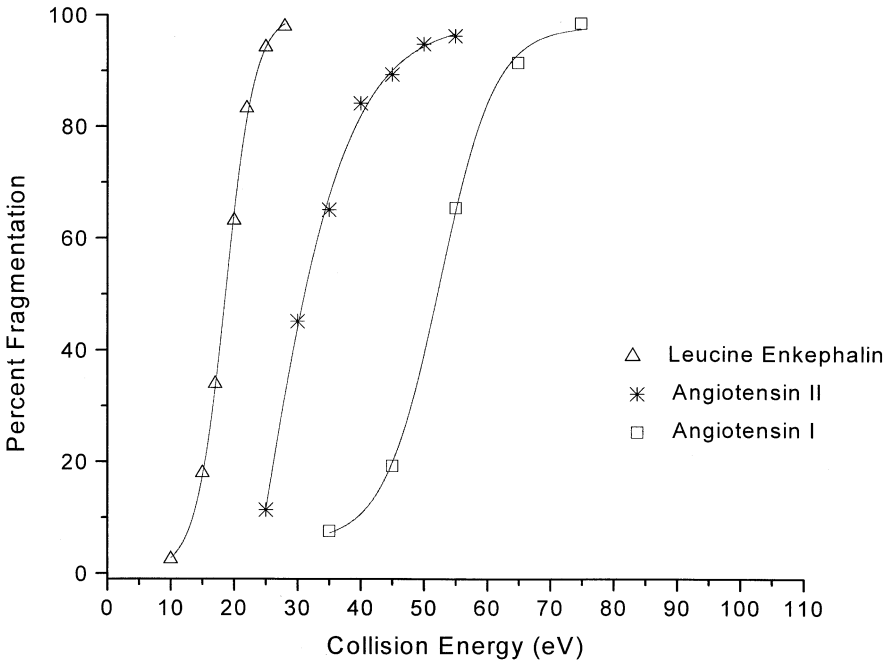

Fig. 9. FAB-SID (surface-induced dissociation) fragmentation efficiency curves for singly protonated oligopeptides (Leucine Enkephalin, YGGFL; Angiotensin II, DRVYIHPF; and Angiotensin I, DRVYIHPFHL). All curves were obtained by using fluorinated surface in the sector-time-of-flight-SID instrument.

ment ions. A mass accuracy of ±0.4 u is achievable for CID fragments, but it was found to be better for SID fragments (±0.1 u) because the parabolic field is used only for acceleration, not kinetic energy focusing, of the product ions. Comparative experiments have shown that, for protonated peptides, the SID sensitivity (on SAM surfaces) is higher by about a single order of magnitude than that of the CID sensitivity. The promising results presented in this article suggest that it is worthwhile to invest future effort in the implementation of SID in a commercial TOF system.

References

[1] R. Cotter, Time-of-Flight Mass Spectrometry: Instrumentation and Applications in Biological Research, American Chemical Society 1997.
[2] M. Guilhaus, V. Mlynski, D. Selby, Rapid Commun Mass Spectrom 11 (1997) 951.
[3] D.H. Russell, R.D. Edmondson, J. Mass Spectrom. 32 (1997) 263.
[4] F. Hillenkamp, J. Karas, R.C. Beavis, B.T. Chait, Anal. Chem. (1991) 63 1193A.
[5] R.G. Cooks, T. Ast, A. Mabud, Int. J. Mass Spectrom. Ion Processes 100 (1990) 209.
[6] K.L. Busch, G.L. Glish, S.A. McLuckey, Mass Spectrometry/Mass Spectromety: Techniques and Application of Tandem Mass Spectrometry, VCH, New York 1988.
[7] S.A. McLuckey, J. Am. Soc. Mass Spectrom. 3 (1992) 599.
[8] R.G. Cooks, J. Mass Spectrom. 30 (1995) 1215.
[9] E. de Hoffmann, J. Mass Spectrom. 31 (1996) 129.
[10] A.R. Dongre, A. Somogyi, V.H. Wysocki, J. Mass Spectrom. 31 (1996) 339.
[11] E. Clayton, R.H. Bateman, Rapid Comm. Mass Spectrom. 6 (1992) 719.
[12] R.H. Bateman, M.R. Green, G. Scott, E. Clayton, Rapid Comm. Mass Spectrom. 9 (1995) 1227.
[13] K.F. Medzihraszky, G.W. Adams, A.L. Burlingame, R.H. Bateman, M.R. Green, J. Am. Soc. Mass Spectrom. 7 (1996) 1.
[14] T. Keough, M.P. Lacey, M.M. Ketcha, R.H. Bateman, M.R. Green, Rapid Comm. Mass Spectrom. 11 (1997) 1702.
[15] A.T. Jackson, R.C.K. Jennings, J.H. Scrivens, M.R. Green, R.H. Bateman, Rapid Comm. Mass Spectrom. 12 (1998) 1914.
[16] R.J. Cotter, T.J. Cornish, B. Musselman, Rapid Comm. Mass Spectrom. 8 (1994) 339.
[17] U.N. Andersen, A.W. Colburn, A.A. Makarov, E.N. Raptakis,

D.J. Reynolds, P.J. Derrick, S.C. Davis, A.D. Hoffman, S. Thomson, Rev. Sci. Instrum. 69 (1998) 1650.
[18] A.R. Bottrill, A.E. Giannakopulos, C. Waterson, D.M. Haddleton, K.S. Lee, P.J. Derrick, Anal. Chem. 71 (1999) 3637.
[19] C. Mair, T. Fiegele, F. Biasioli, R. Wörgötter, V. Grill, M. Lezius, T.D. Märk, Plasma Sources Sci. Technol. 8 (1999) 191.
[20] C. Mair, T. Fiegele, F. Biasioli, T.D. Märk, Eur. Phys. J. D 9 (1999) 551.
[21] A. Rockwood, in The 34th ASMS Conference on Mass Spectrometry and Allied Topics, Cincinnati, OH, 1986.
[22] A.A. Makarov, E.N. Raptakis, P.J. Derrick, Int. J. Mass Spectom. Ion Processes 146 (1995) 165.
[23] G. Tsaprailis, H. Nair, A. Somogyi, V.H. Wysocki, W. Zhong, J.H. Futrell, S.G. Summerfield, S.J. Gaskell, J. Am. Chem. Soc. 121 (1999) 5142.
[24] D.S. Cornett, M. Peschke, K. LaiHing, P.Y. Cheng, K.F. Willey, M.A. Duncan, Rev. Sci. Instrum. 63 (1992) 2177.
[25] D.G. Schultz, H. Lim, S. Garbis, L. Hanley, J. Mass Spectrom. 34 (1999) 217.
[26] J. Jones, Ph.D. dissertation, Virginia Commonwealth University, Richmond, 1995.
[27] A.L. McCormack, Á. Somogyi, A.R. Dongré, V. H. Wysocki, Anal. Chem. 65 (1993) 2859.
[28] J.L. Jones, A.R. Dongré, Á. Somogyi, V.H. Wysocki, J. Am. Chem. Soc. 116 (1994) 8368.
[29] Á. Somogyi, T.E. Kane, V.H. Wysocki, Org. Mass Spectrom. 28 (1993) 283.
[30] Á. Somogyi, T.E. Kane, J.M. Ding, V.H. Wysocki, J. Am. Chem. Soc. 115 (1993) 5275.
[31] M.J. Hayward, F.D.S. Park, L.M. Manzella, S.L. Bernasek, Á. Somogyi, V.H. Wysocki, J. Am. Chem. Soc. 118 (1996) 8375.
[32] M.S. Kim, C.H. Kwon, J.C. Choe, J. Chem. Phys. 113 (2000) 9532.
[33] T.E. Kane, Á. Somogyi, V.H. Wysocki, Org. Mass Spectrom. 28 (1993) 1665.
[34] A.R. Dongré, J.L. Jones, Á. Somogyi, V.H. Wysocki, J. Am. Chem. Soc. 118 (1996) 8365.